

11

Momentum measurement and muon detection

I think that a particle must have a separate reality independent of the measurements. That is, an electron has spin, location, and so forth even when it is not being measured. I like to think that the moon is there even if I am not looking at it.

Albert Einstein

Momentum measurement and, in particular, muon detection is an important aspect of any experiment of particle physics, astronomy or astrophysics. Ultra-high-energy cosmic rays are currently at the forefront of astroparticle physics searching for the accelerators in the sky. These questions can be studied by the detection of extensive air showers at ground level by measuring secondary electrons, muons and hadrons produced by primary cosmic rays which initiate hadronic cascades in the Earth's atmosphere. The detectors have to operate for many years in order to map the galactic sources of high-energy cosmic rays which may be visible at the experimental sites. There are several experiments dedicated to studying these air showers that employ large detector arrays for electron and muon detection. Apart from water Cherenkov and scintillation counters, typical detectors such as limited streamer tubes [1] and resistive-plate chambers are also used [2].

In the field of high energy physics, over the last several decades many outstanding discoveries have been made from the studies of muons along with other precision measurements of leptons and hadrons. Notable are the determination of the number of neutrino generations by the LEP detectors, charm production (J/ψ), the observation of the electroweak bosons (W^\pm, Z), and the top quark (t). Although these particles have higher branching ratios for their hadronic decay channels, it is difficult to measure and isolate hadrons. At the time of the writing of this book – the Large Hadron Collider is under construction (at CERN,

Geneva) – advances in the understanding of the Standard Model of particle physics have led to believe that the physics of Higgs particles as well as new phenomena, like supersymmetry, should show up at a mass scale of approximately a few TeV. ATLAS, CMS, ALICE and LHCb are experiments having large, i.e. several thousand square metres of muon-detection surfaces to signal the presence of new physics. Also precision experiments like Belle and BaBar looking into B physics have to rely on efficient muon identification and accurate momentum measurement. Muons can be identified by the large penetrating power and the relevant parameters to be measured very precisely are energy and momentum. Energies of muons beyond the TeV range can be measured with calorimetric techniques, because the energy loss at high energies is dominated by bremsstrahlung and direct electron-pair production, both of which processes are proportional to the muon energy.

The momenta of muons, just as for all charged particles, are usually determined in magnetic spectrometers. The Lorentz force causes the particles to follow circular or helical trajectories around the direction of the magnetic field. The bending radius of particle tracks is related to the magnetic field strength and the momentum component of the particle perpendicular to the magnetic field. Depending on the experimental situation, different magnetic spectrometers are used.

11.1 Magnetic spectrometers for fixed-target experiments

The basic set-up of a *magnetic spectrometer* for fixed-target experiments (in contrast to storage-ring experiments) is sketched in Fig. 11.1. Particles

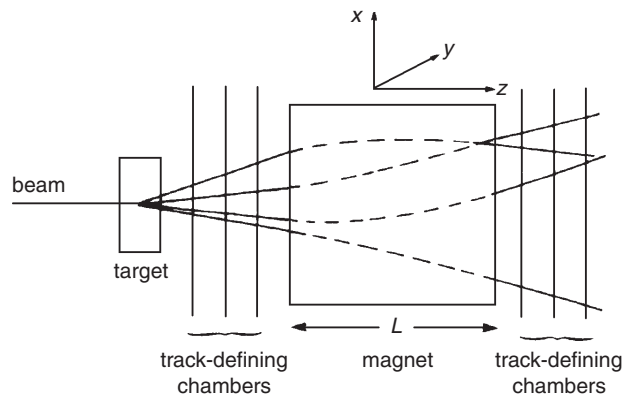


Fig. 11.1. Schematic representation of a magnetic spectrometer in a fixed-target experiment with a stationary target.

of known identity and also, in general, of known energy are incident on a target thereby producing secondary particles in an interaction. The purpose of the spectrometer is to measure the momenta of the charged secondary particles.

Let the magnetic field B be oriented along the y axis, $\vec{B} = (0, B_y, 0)$, whereas the direction of incidence of the primary particles is taken to be parallel to the z axis. In hadronic interactions typical *transverse momenta* of

$$p_T \approx 350 \text{ MeV}/c \tag{11.1}$$

are transferred to secondary particles, where

$$p_T = \sqrt{p_x^2 + p_y^2} . \tag{11.2}$$

Normally, $p_x, p_y \ll p_z$, where the momenta of outgoing particles are described by $\vec{p} = (p_x, p_y, p_z)$. The trajectories of particles incident into the spectrometer are determined in the most simple case by track detectors before they enter and after they have left the magnet. Since the magnetic field is oriented along the y axis, the deflection of charged particles is in the xz plane. Figure 11.2 sketches the track of a charged particle in this plane.

The Lorentz force provides a centripetal acceleration v^2/ρ directed along the bending radius. We choose our coordinate system in such a way that the particles incident into the spectrometer are parallel to the z axis, i.e. $|\vec{p}| = p_z = p$, where \vec{p} is the momentum of the particle to be

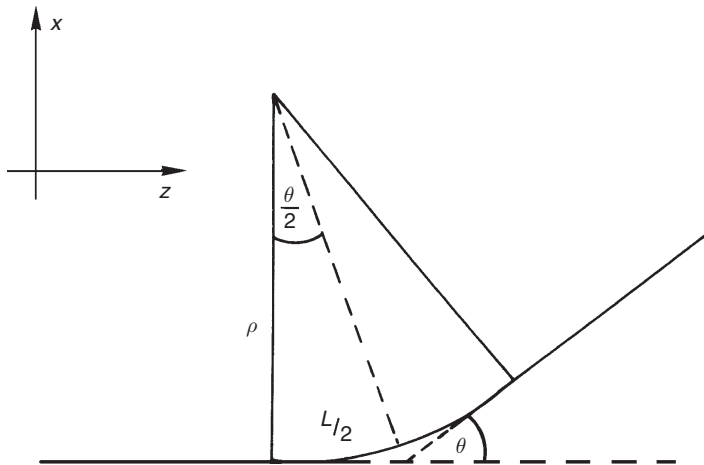


Fig. 11.2. Trajectory of a charged particle in a magnet.

measured. One then has (for $\vec{p} \perp \vec{B}$, where m – mass, v – velocity and ρ – bending radius of the track in the magnetic field):

$$\frac{mv^2}{\rho} = e v B_y . \quad (11.3)$$

The *bending radius* ρ itself is obtained from Eq. (11.3) by

$$\rho = \frac{p}{eB_y} . \quad (11.4)$$

With standard units, which are common in particle and astroparticle physics, this formula leads to

$$\rho \text{ [m]} = \frac{p \text{ [GeV}/c]}{0.3 B \text{ [T]}} . \quad (11.5)$$

The particles pass through the magnet following a circular trajectory, where the bending radius ρ , however, is normally very large compared to the magnet length L . Therefore, the deflection angle θ can be approximated by

$$\theta = \frac{L}{\rho} = \frac{L}{p} e B_y . \quad (11.6)$$

Because of the magnetic deflection, the charged particles obtain an additional transverse momentum of

$$\Delta p_x = p \cdot \sin \theta \approx p \cdot \theta = L e B_y . \quad (11.7)$$

If the magnetic field varies along L , Eq. (11.7) is generalised to

$$\Delta p_x = e \int_0^L B_y(l) dl . \quad (11.8)$$

The accuracy of the momentum determination is influenced by a number of different effects. Let us first consider the influence of the finite track resolution of the detector on the momentum determination. Using Eqs. (11.4) and (11.6), we obtain

$$p = e B_y \cdot \rho = e B_y \cdot \frac{L}{\theta} . \quad (11.9)$$

Since the tracks of ingoing and outgoing particles are straight, the deflection angle θ is the actual quantity to be measured. Because of

$$\left| \frac{dp}{d\theta} \right| = e B_y L \cdot \frac{1}{\theta^2} = \frac{p}{\theta} , \quad (11.10)$$

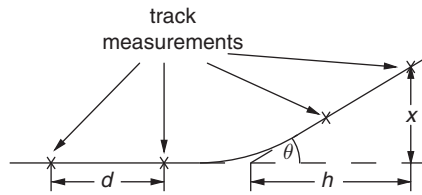


Fig. 11.3. Sketch illustrating the determination of the track measurement error.

one has

$$\frac{dp}{p} = \frac{d\theta}{\theta} \tag{11.11}$$

and

$$\frac{\sigma(p)}{p} = \frac{\sigma(\theta)}{\theta} . \tag{11.12}$$

Let us assume that to determine the deflection angle, θ_{def} , four track coordinates are measured, i.e. two in front of and two behind the magnet (although for a circular orbit three coordinates would in principle be sufficient). If the distance between the sensors in each pair is d (Fig. 11.3), then the input, output and deflection angles are expressed as:

$$\vartheta_{\text{in}} \approx \frac{x_2 - x_1}{d} , \quad \vartheta_{\text{out}} \approx \frac{x_4 - x_3}{d} , \tag{11.13}$$

$$\theta_{\text{def}} = \vartheta_{\text{out}} - \vartheta_{\text{in}} \approx \frac{x_2 - x_1 - x_4 + x_3}{d} . \tag{11.14}$$

If all track measurements have the same measurement error $\sigma(x)$, the variance of the deflection angle is obtained to be

$$\sigma^2(\theta) \propto \sum_{i=1}^4 \sigma_i^2(x) = 4\sigma^2(x) , \tag{11.15}$$

and

$$\sigma(\theta) = \frac{2\sigma(x)}{d} . \tag{11.16}$$

Using Eq. (11.12), this leads to

$$\frac{\sigma(p)}{p} = \frac{2\sigma(x)}{d} \frac{p}{LeB_y} = \frac{p \text{ [GeV/c]}}{0.3 L \text{ [m]}} B \text{ [T]} \cdot \frac{2\sigma(x)}{d} . \tag{11.17}$$

From Eq. (11.17) one sees that the *momentum resolution* $\sigma(p)$ is proportional to p^2 . Taking as an example $L = 1$ m, $d = 1$ m, $B = 1$ T and $\sigma_x = 0.2$ mm, we get

$$\frac{\sigma(p)}{p} = 1.3 \cdot 10^{-3} p \text{ [GeV/c]} . \quad (11.18)$$

Depending on the quality of the track detectors, one may obtain

$$\frac{\sigma(p)}{p} = (10^{-3} \text{ to } 10^{-4}) \cdot p \text{ [GeV/c]} . \quad (11.19)$$

In cosmic-ray experiments, it has become usual practice to define a *maximum detectable momentum* (mdm). This is defined by

$$\frac{\sigma(p_{\text{mdm}})}{p_{\text{mdm}}} = 1 . \quad (11.20)$$

For a magnetic spectrometer with a momentum resolution given by Eq. (11.19), the maximum detectable momentum would be

$$p_{\text{mdm}} = 1 \text{ TeV/c to } 10 \text{ TeV/c} . \quad (11.21)$$

The momentum measurement is normally performed in an *air-gap magnet*. The effect of multiple scattering is low in this case and influences the measurement accuracy only at low momenta. Because of the high penetrating power of muons, their momenta can also be analysed in *solid-iron magnets*. For this kind of application, however, the influence of multiple scattering cannot be neglected.

A muon penetrating a solid-iron magnet of thickness L obtains a transverse momentum $\Delta p_{\text{T}}^{\text{MS}}$ due to multiple scattering according to

$$\Delta p_{\text{T}}^{\text{MS}} = p \cdot \sin \theta_{\text{rms}} \approx p \cdot \theta_{\text{rms}} = 19.2 \sqrt{\frac{L}{X_0}} \text{ MeV/c} \quad (11.22)$$

(Fig. 11.4 and Eq. (1.53) for $p \gg m_0c$ and $\beta \approx 1$).

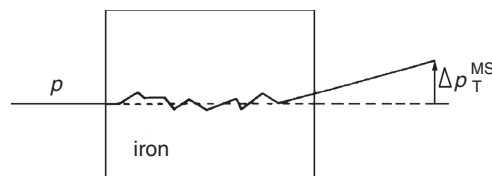


Fig. 11.4. Illustration of the multiple-scattering error.

Since the magnetic deflection is in the x direction, only the multiple-scattering error projected onto this direction is of importance:

$$\Delta p_x^{\text{MS}} = \frac{19.2}{\sqrt{2}} \sqrt{\frac{L}{X_0}} \text{ MeV}/c = 13.6 \sqrt{\frac{L}{X_0}} \text{ MeV}/c . \quad (11.23)$$

The momentum resolution limited by the effect of multiple scattering is given by the ratio of the deflection by multiple scattering to the magnetic deflection according to [3]

$$\left. \frac{\sigma(p)}{p} \right|^{\text{MS}} = \frac{\Delta p_x^{\text{MS}}}{\Delta p_x^{\text{magn}}} = \frac{13.6 \sqrt{L/X_0} \text{ MeV}/c}{e \int_0^L B_y(l) dl} . \quad (11.24)$$

Both the deflection angle θ caused by the Lorentz force and the multiple-scattering angle are inversely proportional to the momentum. Therefore, the momentum resolution in this case does not depend on the momentum of the particle.

For solid-iron magnetic spectrometers ($X_0 = 1.76 \text{ cm}$) typical values of $B = 1.8 \text{ T}$ are used, leading to a momentum resolution of, see Eq. (11.24),

$$\left. \frac{\sigma(p)}{p} \right|^{\text{MS}} = 0.19 \cdot \frac{1}{\sqrt{L [\text{m}]} } . \quad (11.25)$$

This gives for $L = 3 \text{ m}$

$$\left. \frac{\sigma(p)}{p} \right|^{\text{MS}} = 11\% . \quad (11.26)$$

This equation only contains the effect of *multiple scattering* on the momentum resolution. In addition, one has to consider the momentum-measurement error from the uncertainty of the position measurement. This error can be obtained from Eq. (11.17) or from the determination of the *sagitta* (Fig. 11.5) [4]. The sagitta s is related to the magnetic bending radius ρ and the magnetic deflection angle θ by

$$s = \rho - \rho \cos \frac{\theta}{2} = \rho \left(1 - \cos \frac{\theta}{2} \right) . \quad (11.27)$$

Because of $1 - \cos \frac{\theta}{2} = 2 \sin^2 \frac{\theta}{4}$, one obtains

$$s = 2\rho \sin^2 \frac{\theta}{4} . \quad (11.28)$$

Since $\theta \ll 1$, the sagitta can be approximated by (θ in radians)

$$s = \frac{\rho \theta^2}{8} . \quad (11.29)$$

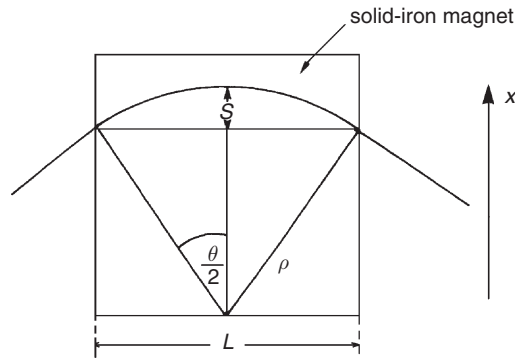


Fig. 11.5. Illustration of the sagitta method for momentum determination [4].

In the following we will replace B_y by B for simplicity. Using Eqs. (11.9) and (11.4) for θ and ρ the sagitta can be expressed by

$$s = \frac{\rho}{8} \cdot \left(\frac{eBL}{p} \right)^2 = \frac{eBL^2}{8p} . \quad (11.30)$$

For fixed units one gets

$$s \text{ [m]} = 0.3 B \text{ [T]} (L \text{ [m]})^2 / (8p \text{ [GeV}/c]) . \quad (11.31)$$

The determination of the sagitta requires at least 3 position measurements x_i ($i = 1, 2, 3$). These can be obtained from 3 tracking detectors positioned at the entrance (x_1) and at the exit (x_3) of the magnet, while one chamber could be placed in the centre of the magnet (x_2). Because of

$$s = x_2 - \frac{x_1 + x_3}{2} \quad (11.32)$$

and under the assumption that the *track measurement errors* $\sigma(x)$ are the same for all chambers, it follows that

$$\sigma(s) = \sqrt{\frac{3}{2}} \sigma(x) . \quad (11.33)$$

This leads to a momentum resolution from track measurement errors of

$$\frac{\sigma(p)}{p} \Big|_{\text{track error}} = \frac{\sigma(s)}{s} = \frac{\sqrt{\frac{3}{2}} \sigma(x) \text{ [m]} \cdot 8p \text{ [GeV}/c]}{0.3 B \text{ [T]} (L \text{ [m]})^2} . \quad (11.34)$$

If the track is measured not only at 3 but at N points equally distributed over the magnet length L , it can be shown that the momentum resolution due to the finite track measurement error is given by [5]

$$\left. \frac{\sigma(p)}{p} \right|_{\text{track error}} = \frac{\sigma(x) \text{ [m]}}{0.3 B \text{ [T]} (L \text{ [m]})^2} \sqrt{720/(N + 4)} \cdot p \text{ [GeV/c]} . \quad (11.35)$$

For $B = 1.8 \text{ T}$, $L = 3 \text{ m}$, $N = 4$ and $\sigma(x) = 0.5 \text{ mm}$ Eq. (11.35) leads to

$$\left. \frac{\sigma(p)}{p} \right|_{\text{track error}} \approx 10^{-3} \cdot p \text{ [GeV/c]} . \quad (11.36)$$

If the N measurements are distributed over L in k constant intervals, one has

$$L = k \cdot N \quad (11.37)$$

and thereby (if $N \gg 4$):

$$\left. \frac{\sigma(p)}{p} \right|_{\text{track error}} \propto (L \text{ [m]})^{-5/2} \cdot (B \text{ [T]})^{-1} \cdot p \text{ [GeV/c]} . \quad (11.38)$$

To obtain the total error on the momentum determination, the multiple-scattering and track-resolution error have to be combined. Both contributions according to Eqs. (11.26) and (11.36) are plotted in Fig. 11.6 for the

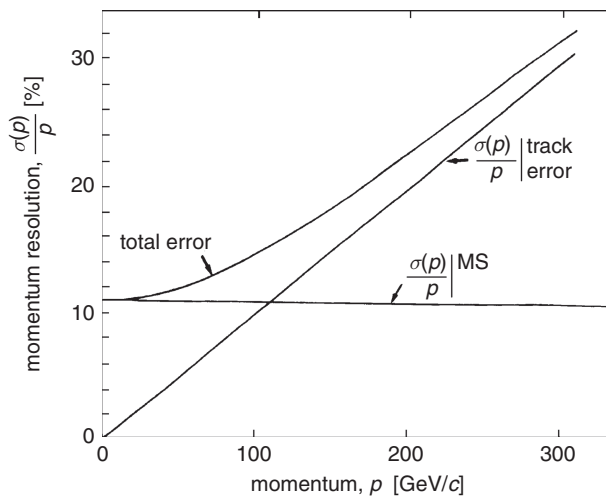


Fig. 11.6. Contributions to the momentum resolution for a solid-iron magnetic spectrometer.

aforementioned parameters of a solid-iron magnetic spectrometer. At low momenta multiple scattering dominates the error and at high momenta it is limited by the track measurement error.

For an air-gap magnet the error contribution due to multiple scattering is naturally much smaller. If Eq. (11.24) is applied to an air-gap magnet, ($X_0 = 304\text{ m}$), one obtains

$$\left. \frac{\sigma(p)}{p} \right|_{\text{MS}} = 1.4 \cdot 10^{-3} / \sqrt{L [\text{m}]}, \quad (11.39)$$

which means for $L = 3\text{ m}$:

$$\left. \frac{\sigma(p)}{p} \right|_{\text{MS}} = 0.08\% . \quad (11.40)$$

For a realistic experiment one has to consider another effect that will degrade the momentum resolution of muons. In particular, at high energies muons will undergo electromagnetic interactions, sometimes with large energy transfers, in the solid-iron magnet, like bremsstrahlung and direct electron-pair production. In addition, muons can undergo photonuclear interactions. A monoenergetic muon beam will develop a ‘radiative tail’ due to bremsstrahlung and pair-production losses. The probability for an energy transfer of more than 10 GeV for a 200 GeV muon in a 2 m long iron magnet is already 3% [6]. This increases to 12% for a 1 TeV muon in 2 m of iron [7]. The secondaries produced by a muon might also emerge from the solid-iron magnet, thereby complicating the track reconstruction of the deflected muon. In rare cases also muon-trident production can occur, i.e.

$$\mu + \text{nucleus} \rightarrow \mu + \mu^+ + \mu^- + \text{nucleus}' . \quad (11.41)$$

Figure 11.7 shows such a process initiated by an energetic cosmic-ray muon in the ALEPH detector.

In such a case it would even be difficult to find the correct outgoing muon.

11.2 Magnetic spectrometers for special applications

Fixed-target experiments have the advantage that *secondary beams* can be produced from a primary target. These secondary beams can consist of many types of different particles so that one can perform experiments with, e.g. neutrino, muon, photon or K_L^0 beams. The disadvantage with fixed-target experiments, however, is that the available centre-of-mass energy is relatively small. Therefore, investigations in the field of

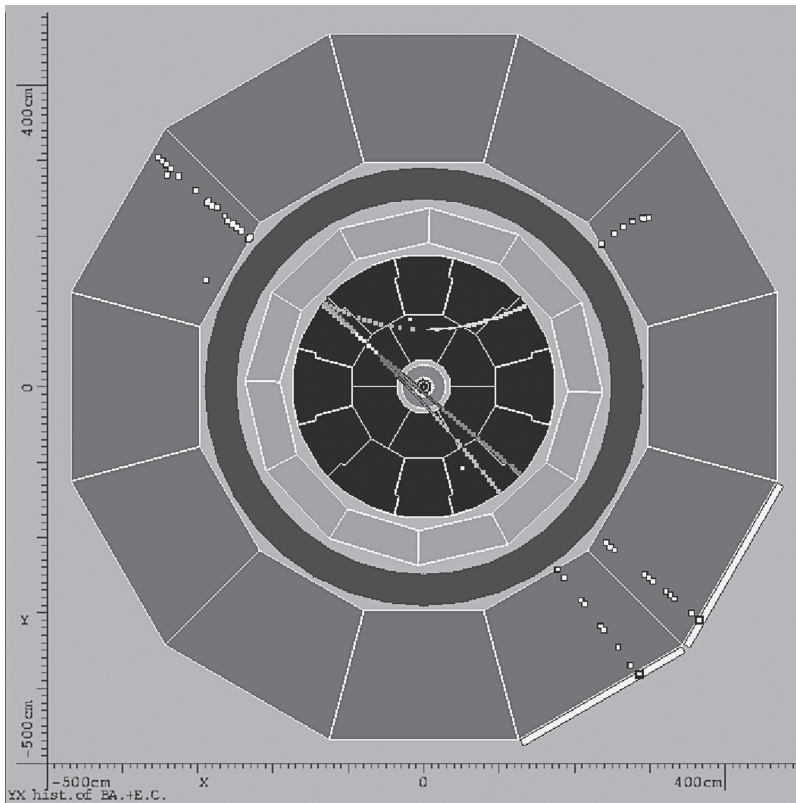


Fig. 11.7. Cosmic-ray muon undergoing a muon-trident production in the ALEPH detector. The muon pair is created in the flux return of the solenoidal magnetic field. The bending of one of the secondary muons in the iron is seen to be opposite to the bending in the central detector [8].

high energy physics are frequently done at storage rings. In storage-ring experiments, the centre-of-mass system is identical with the laboratory system (for a crossing angle of zero), if the colliding beams have the same energy and are opposite in momentum. The event rates are in general rather low because the target density – one beam represents the target for the other and vice versa – is low compared to fixed-target experiments. There are, however, important differences between collider and fixed-target experiments: in the first case the interaction products are emitted into the full solid angle, while in the latter case the products are released within a narrow cone around the incident direction. Therefore – in contrast to fixed-target experiments – storage-ring detectors normally have to cover the full solid angle of 4π surrounding the interaction point. Such a *hermeticity* allows a complete reconstruction of individual events.

Depending on the type of storage ring, different magnetic-field configurations can be considered.

For proton–proton (or $p\bar{p}$) storage rings *dipole magnets* can be used, where the magnetic field is perpendicular to the beam direction. Since such a dipole also bends the stored beam, its influence must be corrected by compensation coils. The compensation coils are also dipoles, but with opposite field gradient, so that there is no net effect on the stored beams. Such a configuration is rarely used for electron–positron storage rings – except at relatively low energies [9] – because the strong dipole field would cause the emission of intense synchrotron radiation, which cannot be tolerated for the storage-ring operation and the safe running of the detectors.

A dipole magnet can be made self-compensating if two dipoles with opposite field gradient on both sides of the interaction point are used instead of only one dipole. Compensation is automatically fulfilled in this case, but at the expense of strongly inhomogeneous magnetic fields at the interaction point which complicate the track reconstruction considerably. If, on the other hand, *toroidal magnets* are employed, one can achieve that the beams traverse the spectrometer in a region of zero field. Multiple scattering, however, on the inner cylinder of the toroidal magnet limits the momentum resolution.

In most cases a *solenoidal magnetic field* is chosen, in which the stored beams run essentially – apart from small beam crossing angles or betatron oscillations – parallel to the magnetic field (like in Fig. 11.7 [8]). Therefore, the detector magnet has no influence on the beams, and also no or very little synchrotron radiation is produced. In either case one has to consider that any magnetic spectrometer used in the detector becomes an integral element of the accelerator and should be properly accounted for and compensated.

The track detectors are mounted inside the magnetic coil and are therefore also cylindrical. The longitudinal magnetic field acts only on the transverse momentum component of the produced particles and leads to a momentum resolution given by Eq. (11.35), where $\sigma(x)$ is the coordinate resolution in the plane perpendicular to the beam axis. Figure 11.8 shows schematically two tracks originating from the interaction point in a projection perpendicular to the beam ($r\varphi$ plane) and parallel to the beam (rz plane). The characteristic track parameters are given by the polar angle θ , the azimuthal angle φ and the radial coordinate r , i.e. the distance from the interaction point. A sketch of a simulated muon-track reconstruction in the Compact Muon Solenoid (CMS) at CERN is shown in Fig. 11.9 [10]. A simulated event of the production of supersymmetric particles in the ATLAS experiment with two muons escaping to the left can be seen in Fig. 11.10 [11].

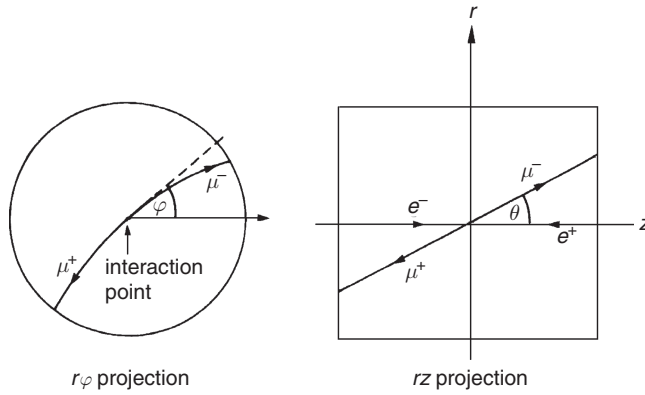


Fig. 11.8. Track reconstruction in a solenoid detector (shown for an event $e^+e^- \rightarrow \mu^+\mu^-$).

If N coordinates are measured along a track of total length L with an accuracy of $\sigma_{r\varphi}$ in a magnetic field B , the transverse momentum resolution caused by the track measurement error is found to be [5], see Eq. (11.35),

$$\frac{\sigma(p)}{p_T} \Big|_{\text{track error}} = \frac{\sigma_{r\varphi} \text{ [m]}}{0.3 B \text{ [m]} (L \text{ [m]})^2} \sqrt{\frac{720}{N+4}} \cdot p_T \text{ [GeV}/c] . \quad (11.42)$$

In addition to the track error one has to consider the multiple-scattering error. This is obtained from Eq. (11.24) for the general case of also non-relativistic velocities β as

$$\frac{\sigma(p)}{p_T} \Big|_{\text{MS}} = 0.045 \frac{1}{\beta} \frac{1}{B \text{ [T]} \sqrt{L \text{ [m]} X_0 \text{ [m]}}} , \quad (11.43)$$

where X_0 is the average radiation length of the material traversed by the particle.

The total momentum of the particle is obtained from p_T and the polar angle θ to be

$$p = \frac{p_T}{\sin \theta} . \quad (11.44)$$

As in the transverse plane, the measurement of the polar angle contains a track error and multiple-scattering error.

If the z coordinate in the track detector is determined with an accuracy $\sigma(z)$, the error on the measurement of the polar angle can be derived from a simple geometrical consideration to be

$$\sigma(\theta) = \sin^2(\theta) \frac{\sigma(z)}{r} = \sin(2\theta) \frac{\sigma(z)}{2z} . \quad (11.45)$$

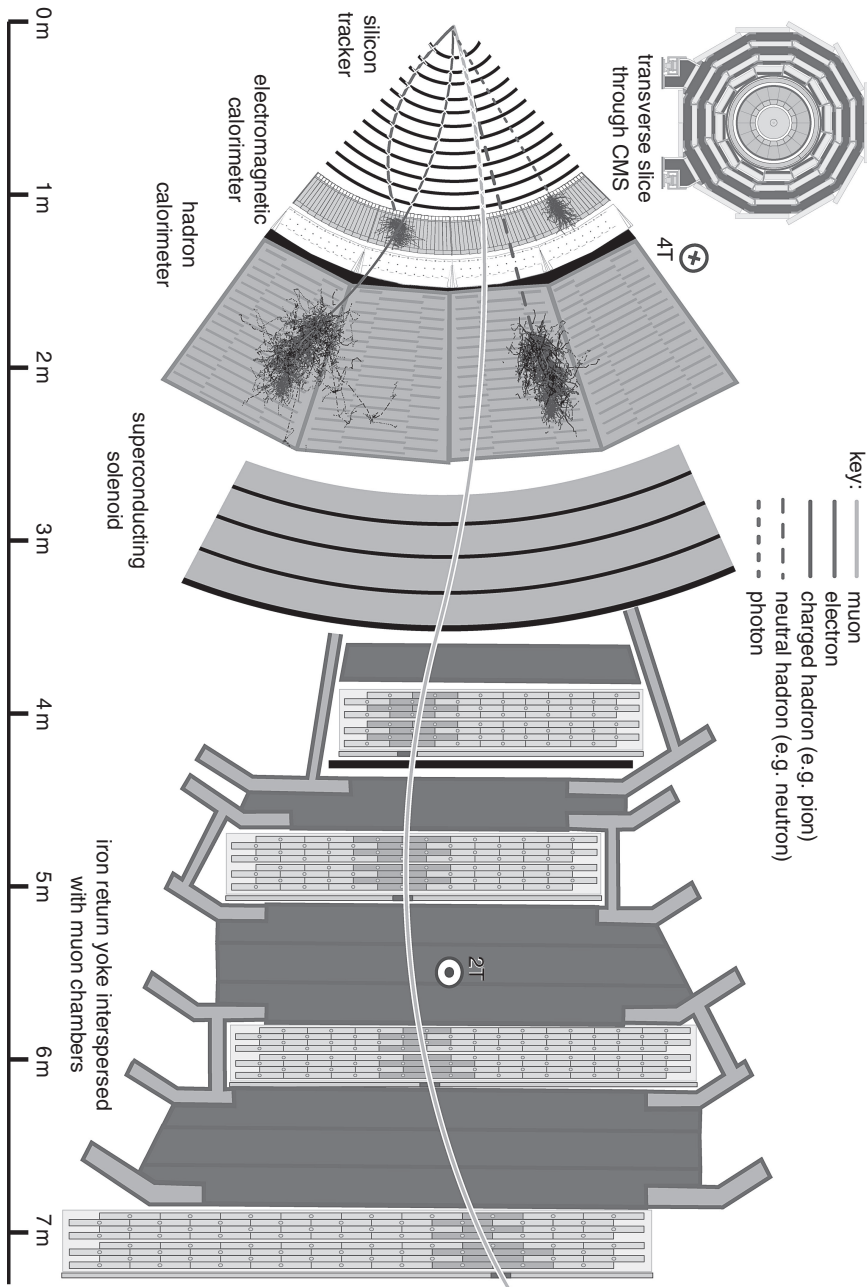


Fig. 11.9. Sketch demonstrating the particle-identification possibilities in the CMS experiment at CERN. A muon originating from the vertex is deflected in the central solenoidal magnet. The backbending of the muon is clearly visible in the outer magnetic spectrometer [10].

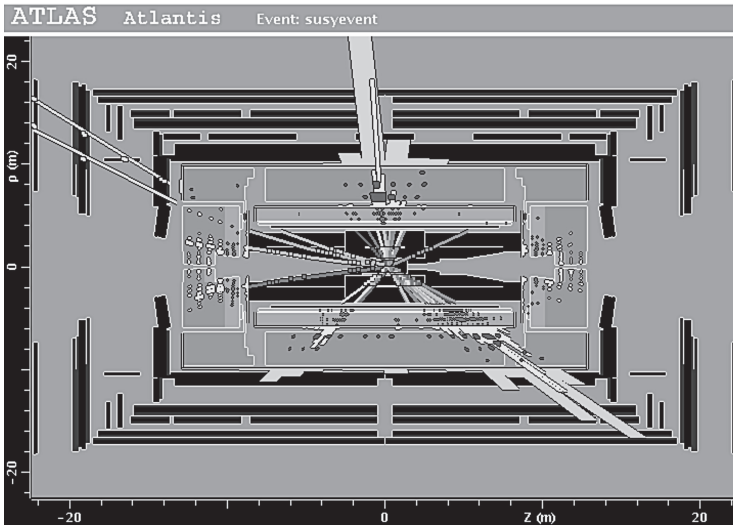


Fig. 11.10. Event simulation for the production of supersymmetric particles in ATLAS and reconstruction of the tracks in the various subdetector components with two energetic muons escaping to the left [11]. The central part of ATLAS incorporates a solenoidal field, while the outer section of the experiment uses toroidal magnets.

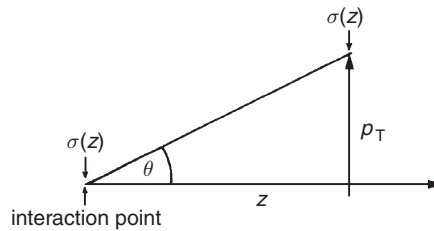


Fig. 11.11. Illustration of the polar-angle measurement error for the case of only two coordinates, defining a track. p_T is the transverse momentum to the beam.

(For high-energy particles the particle track in the rz plane is a straight line, see Fig. 11.11.) If the particle track is measured in N equidistant steps each with an error $\sigma(z)$ along the track length L , the angular uncertainty is obtained to be [4, 5]

$$\sigma(\theta)|_{\text{track error}} = \frac{\sigma(z)}{L} \sqrt{\frac{12(N-1)}{N(N+1)}}. \quad (11.46)$$

In this formula z is the projected track length in the z direction which is normally on the same order of magnitude as the transverse length of

a track. Equation (11.46) describes only the track measurement error. In addition, one has to consider the multiple-scattering error which can be derived from Eq. (1.50) to be

$$\sigma(\theta)|^{\text{MS}} = \frac{0.0136}{\sqrt{3}} \cdot \frac{1}{p [\text{GeV}/c]} \cdot \sqrt{\frac{l}{X_0}}, \quad (11.47)$$

where l is the track length (in units of radiation lengths) and $\beta = 1$ is assumed. The factor $1/\sqrt{3}$ is motivated in [12, 13].

Gaseous detectors with extremely low transverse mass are generally used in solenoids. Therefore, the momentum measurement error due to multiple scattering plays only a minor rôle. Equation (11.42) shows that the momentum resolution improves with the product BL^2 . It also improves for a fixed track length with the number of track measurement points although only approximately like $1/\sqrt{N}$.

In the past multiwire proportional chambers or drift chambers have been used as particle trackers in muon spectrometers. To cover large areas, streamer tubes with digital readout, muon drift tubes or resistive-plate chambers – often inserted into slots in the magnetised iron – can be used. For experiments at the Large Hadron Collider at CERN momentum resolutions of $\Delta p/p < 10^{-4} \times p/(\text{GeV}/c)$ for $p > 300 \text{ GeV}/c$ are envisaged. Because of their excellent time resolution resistive-plate chambers can also be used for deriving a muon trigger.

11.3 Problems

11.1 What is the average energy loss of 1 TeV muons in a solid-iron magnet of 3 m thickness?

11.2 In gaseous detectors track reconstruction is often hindered by δ electrons which spiral in the magnetic field thus producing many hits. For LHC experiments track multiplicities of 100 charged particles per beam crossing are not uncommon. Low-momentum electrons are not so serious because their helices occupy only a small volume. High-momentum electrons are only slightly deflected. It is the δ rays with bending radii between 5 cm and 20 cm that represent problems.

Estimate the number of δ rays with bending radii between 5 cm and 20 cm in a 3 m-diameter argon-filled track detector at atmospheric pressure for a magnetic field of 2 T. Assume that the charged particles that create δ rays are very energetic ($\gg 10 \text{ GeV}$).

11.3 High-resolution β -ray spectroscopy can be accomplished with a *double-focussing semicircular magnetic spectrometer* [14–16]. The magnetic field in this spectrometer is axially symmetric but inhomogeneous in the radial direction like

$$B(\rho) = B(\rho_0) \left(\frac{\rho_0}{\rho} \right)^n, \quad 0 < n < 1,$$

where ρ_0 is the bending radius of the central orbit. Focussing in radial direction is achieved after an angle of

$$\Theta_\rho = \frac{\pi}{\sqrt{1-n}}$$

and in axial direction after [16]

$$\Theta_\varphi = \frac{\pi}{\sqrt{n}}.$$

- (a) Work out the radial dependence of the guiding field and determine the angle at which double focussing is achieved.
- (b) What kind of average energy loss will a 10 keV electron experience in such a spectrometer ($\rho_0 = 50$ cm, $\frac{dE}{dx}(10 \text{ keV}) = 27$ keV/cm, pressure $p = 10^{-3}$ Torr)? How many ionisation processes would this correspond to?

11.4 Most colliders use magnetic quadrupoles to focus the beam into the interaction point, because a beam of small transverse dimensions ensures high luminosity. The magnetic bending power must be proportional to the distance of the charged particle from the ideal orbit, i.e., particles far away from the central orbit must experience a stronger deflection than those that are already close to the desired orbit.

It has been shown that the bending angle θ depends on the length of the magnetic field, ℓ , and the bending radius ρ like, see Eq. (11.6),

$$\theta = \frac{\ell}{\rho} = \frac{\ell}{p} e B_y \propto x, \quad \text{i.e. } B_y \cdot \ell \propto x,$$

where B_y is the magnetic field strength that causes the focussing in the x direction. In the direction perpendicular to x a bending field B_x is required with the corresponding property

$$\theta \propto B_x \ell \propto y.$$

For practical reasons the length ℓ of the quadrupole is fixed. How has the shape of the iron yoke of the quadrupole to look like so that it produces a magnetic field with the desired properties?

References

- [1] KASCADE-Grande, T. Antoni, A. Bercuci, *et al.*, A Large Area Limited Streamer Tube Detector for the Air Shower Experiment, KASCADE-Grande, *Nucl. Instr. Meth.* **533** (2003) 387–403
- [2] C. Bacci *et al.*, Performance of the RPC's for the ARGO Detector Operated at the YANGBAJING laboratory (4300 m a.s.l.), Prepared for 6th Workshop on Resistive Plate Chambers and Related Detectors (RPC 2001), Coimbra, Portugal, 26–27 November 2001, *Nucl. Instr. Meth.* **A508** (2003) 110–15
- [3] K. Kleinknecht, *Detectors for Particle Radiation*, 2nd edition, Cambridge University Press, Cambridge (1998); *Detektoren für Teilchenstrahlung*, Teubner, Wiesbaden (2005)
- [4] K. Kleinknecht, *Detektoren für Teilchenstrahlung*, Teubner, Stuttgart (1984, 1987, 1992); *Detectors for Particle Radiation*, Cambridge University Press, Cambridge (1986)
- [5] R.L. Glückstern, Uncertainties in Track Momentum and Direction due to Multiple Scattering and Measurement Errors, *Nucl. Instr. Meth.* **24** (1963) 381–9
- [6] R. Baumgart *et al.*, Interaction of 200 GeV Muons in an Electromagnetic Streamer Tube Calorimeter, *Nucl. Instr. Meth.* **A258** (1987) 51–7
- [7] C. Grupen, Electromagnetic Interactions of High Energy Cosmic Ray Muons, *Fortschr. der Physik* **23** (1976) 127–209
- [8] CosmoALEPH Collaboration, F. Maciuc *et al.*, Muon-Pair Production by Atmospheric Muons in CosmoALEPH, *Phys. Rev. Lett.* **96** (2006) 021801, 1–4
- [9] S.E. Baru *et al.*, Experiments with the MD-1 Detector at the e^+e^- Collider VEPP-4 in the Energy Region of Upsilon Mesons, *Phys. Rep.* **267** (1996) 71–159
- [10] CMS Collaboration, <http://cmsinfo.cern.ch/Welcome.html/>; http://cmsinfo.cern.ch/Welcome.html/CMSdocuments/DetectorDrawings/Slice/CMS_Slice.gif
- [11] ATLAS Collaboration: <http://atlantis.web.cern.ch/atlantis/>
- [12] Particle Data Group, Review of Particle Properties, *Phys. Lett.* **239** (1990) 1–516
- [13] Particle Data Group, Review of Particle Properties, *Phys. Rev.* **D45** (1992) 1–574; Particle Data Group, *Phys. Rev.* **D46** (1992) 5210 (Errata)
- [14] K. Siegbahn (ed.), *Alpha, Beta and Gamma-Ray Spectroscopy*, Vols. 1 and 2, Elsevier–North Holland, Amsterdam (1968)
- [15] G. Hertz, *Lehrbuch der Kernphysik*, Bd. 1, Teubner, Leipzig (1966)

- [16] N. Svartholm & K. Siegbahn, An Inhomogeneous Ring-Shaped Magnetic Field for Two-Directional Focusing of Electrons and Its Applications to β -Spectroscopy, *Ark. Mat. Astron. Fys. Ser.* **A33**, Nr. 21 (1946) 1–28; N. Svartholm, The Resolving Power of a Ring-Shaped Inhomogeneous Magnetic Field for Two-Directional Focusing of Charged Particles, *Ark. Mat. Astron. Fys. Ser.* **A33**, Nr. 24 (1946) 1–10; K. Siegbahn & N. Svartholm, Focusing of Electrons in Two Dimensions by an Inhomogeneous Magnetic Field, *Nature* **157** (1946) 872–3; N. Svartholm, Velocity and Two-Directional Focusing of Charged Particles in Crossed Electric and Magnetic Fields, *Phys. Rev.* **74** (1948) 108–9